

Configuration mixing in ^{188}Pb : Band structure and electromagnetic properties

V. Hellemans, R. Fossion, S. De Baerdemacker, and K. Heyde

Department of Subatomic and Radiation Physics, Proeftuinstraat 86, B-9000 Gent, Belgium

(Received 13 October 2004; published 15 March 2005)

In the present paper, we carry out a detailed analysis of the presence and mixing of various families of collective bands in ^{188}Pb . Making use of the interacting boson model, we construct a particular intermediate basis that can be associated with the unperturbed bands used in more phenomenological studies. We use the $E2$ decay to construct a set of collective bands and discuss in detail the $B(E2)$ values. Monopole transition ρ^2 values are calculated. We also perform an analysis of these theoretical results [Q , $B(E2)$] to deduce an intrinsic quadrupole moment and the associated quadrupole deformation parameter, using an axially deformed rotor model.

DOI: 10.1103/PhysRevC.71.034308

PACS number(s): 21.60.Fw, 21.60.Ev

I. INTRODUCTION

Lead isotopes provide a unique laboratory to study the phenomenon of shape coexistence in nuclei [1–4] and have very recently been the subject of much experimental and theoretical interest [5–16]. The combined effect of the proton shell gap at $Z = 82$ for the Pb nuclei and the large number of valence nucleons outside the closed $N = 126$ core (in this case, neutron holes) results in an important lowering of the energy of proton particle-hole excitations [17]. More specifically, near neutron midshell (at $N = 104$), the proton 2p-2h and 4p-4h excitations descend to very low excitation energy because of the very large proton-neutron binding energy that results from the interactions between the core-excited protons across the $Z = 82$ shell closure and the large number of valence neutrons outside the $N = 126$ shell closure. As a consequence, mixing can result among various families of configurations having approximately the same excitation energy. In particular, the lowest lying 0^+ and 2^+ states can become strongly mixed such that it is very difficult to assign a “configuration label” to them. In Sec. II, we succinctly describe the essentials of configuration mixing using the interacting boson model (IBM) [18–20]. In Sec. III we seek to obtain a better understanding of the low-spin collective states and to construct particular bands by following the calculated $E2$ decay starting at the high-spin states in the particular case of ^{188}Pb . In Sec. IV we use the derived wave functions to calculate $E0$ properties. Finally, in Sec. V, we make use of the quadrupole moments and $B(E2)$ values calculated within the framework of the IBM to extract collective model parameters (intrinsic quadrupole moments and quadrupole deformation β_0). Hereby we aim to highlight the equivalence between the IBM approach, used as a highly truncated shell-model calculation, and a geometrical rotational model, as can be derived from mean-field methods [6,8,10,16,21,22].

II. CONFIGURATION MIXING

In a recent study that concentrated on describing intruder bands and configuration mixing in neutron-deficient Pb isotopes, a three-configuration mixing calculation has been performed in the context of the IBM [23]. We refer to that

paper for more details but present succinctly the main points. One can approximate the regular and intruder states as 0p-0h, 2p-2h, and 4p-4h excitations across the $Z = 82$ proton closed shell that interact with the large number of valence neutrons outside of the $N = 126$ neutron closed shell. Within the IBM the Hamiltonian then takes the form

$$\hat{H} = \hat{H}_{\text{reg}} + \hat{H}_{2\text{p-2h}} + \hat{H}_{4\text{p-4h}} + \hat{V}_{\text{mix}}, \quad (1)$$

with

$$\hat{H}_{\text{reg}} = \varepsilon_{\text{reg}} \hat{n}_d + \kappa_{\text{reg}} \hat{Q}_{\text{reg}} \cdot \hat{Q}_{\text{reg}}, \quad (2)$$

$$\hat{H}_i = \varepsilon_i \hat{n}_d + \kappa_i \hat{Q}_i \cdot \hat{Q}_i + \Delta_i, \quad (3)$$

and

$$\hat{V}_{\text{mix}} = \hat{V}_{\text{mix},1} + \hat{V}_{\text{mix},2}, \quad (4)$$

$$\hat{V}_{\text{mix},i} = \alpha_i (s^\dagger \cdot s^\dagger + s \cdot s) + \beta_i (d^\dagger \cdot d^\dagger + \tilde{d} \cdot \tilde{d}) \quad (5)$$

The quadrupole operator \hat{Q}_i is defined as

$$\hat{Q}_i = (s^\dagger \tilde{d} + d^\dagger \tilde{s})^{(2)} + \chi_i (d^\dagger \tilde{d})^{(2)}. \quad (6)$$

For details on the notation we refer to Fossion *et al.* [23]. The diagonalization of the energy matrices, corresponding to the Hamiltonian (1), is carried out in the $U(5)$ basis, expressing the eigenvectors in the $[N] \oplus [N + 2] \oplus [N + 4]$ model space. Unfortunately, using this method, one has no clear insight into the interaction matrix elements coupling the unperturbed states that result from a diagonalization in the separate subspaces $[N]$, $[N + 2]$, and $[N + 4]$, respectively.

So instead of a complete diagonalization of the Hamiltonian matrix, we first rotate into an intermediate basis in which only the separate parts of the Hamiltonian (1) (i.e., \hat{H}_{reg} , $\hat{H}_{2\text{p-2h}}$, and $\hat{H}_{4\text{p-4h}}$) become diagonal. We thus have three different bases:

- the $U(5)$ basis $|J, k\rangle_N$, where J is the angular momentum, N is the number of bosons, and k is the rank number;
- the basis in which the full Hamiltonian (1) is diagonal $|J, i\rangle$; and
- the *intermediate bases* in which the Hamiltonian (1), excluding \hat{V}_{mix} , is diagonal in the three different subspaces $[N]$, $[N + 2]$, and $[N + 4]$; respectively, they are denoted as $|J, l\rangle'_N$, $|J, l\rangle'_{N+2}$, and $|J, l\rangle'_{N+4}$, with l as a rank number.

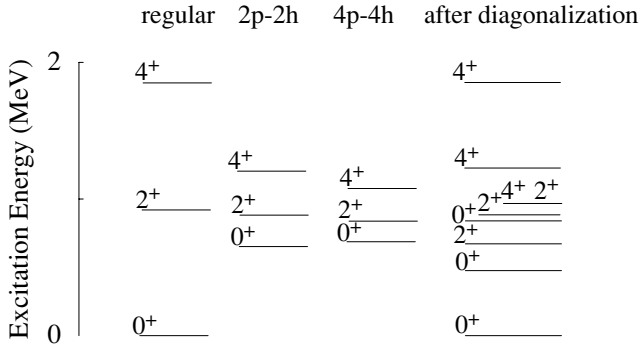


FIG. 1. Low-energy part of the IBM spectrum for ^{188}Pb . The first three configurations taken from the left show the absolute energies for the lowest unperturbed bands. At the extreme right, the IBM spectrum after diagonalization of the full Hamiltonian (1) is shown.

These bases are connected in the following way. The basis in which the full Hamiltonian is diagonal [expressed in the $U(5)$ basis] reads

$$\begin{aligned}
 |J, i\rangle = & \sum_{k=1}^{\dim_N} a_{k,i}^N(J) |J, k\rangle_N \\
 & + \sum_{l=\dim_N+1}^{\dim_N+\dim_{N+2}} a_{l,i}^{N+2}(J) |J, l\rangle_{N+2} \\
 & + \sum_{m=\dim_N+\dim_{N+2}+1}^{\dim_N+\dim_{N+2}+\dim_{N+4}} a_{m,i}^{N+4}(J) |J, m\rangle_{N+4}, \quad (7)
 \end{aligned}$$

and the “intermediate” basis becomes

$$|J, l\rangle'_N = \sum_{k=1}^{\dim_N} b_{k,l}^N(J) |J, k\rangle_N, \quad (8)$$

(and similarly for $N+2$ and $N+4$). In these equations \dim_N , \dim_{N+2} , and \dim_{N+4} are the dimensions of the corresponding configuration spaces for a certain angular momentum J containing N , $N+2$, and $N+4$, bosons, respectively. The matrix \mathbf{B}^N diagonalizes the configuration with N bosons and the matrix \mathbf{A} diagonalizes the full Hamiltonian (1) directly (the indices N , $N+2$, and $N+4$ for matrix \mathbf{A} are added for the sake of clearness). We omit the dimensions of the summations from now on.

Rotation of the Hamiltonian matrix expressed in the $U(5)$ basis into the “intermediate” basis results in the energy levels of a set of bands in the $0p-0h$, $2p-2h$, and $4p-4h$ subspaces separately (see also the three spectra in the left part in Fig. 1). These bands correspond to the unperturbed bands that are extracted in phenomenological calculations as carried out by Dracoulis *et al.* [9], Allatt *et al.* [24], and Page *et al.* [25]. From now on we will call the energy levels (bands) resulting from rotation of the Hamiltonian matrix into the intermediate basis unperturbed levels (bands) to avoid confusion and we will denote them as the $|J, l\rangle'_N$ states [see Eq. (8)].

By calculating the mixing matrix elements of \hat{V}_{mix} in this intermediate basis, we obtain the mixing matrix elements for

TABLE I. IBM parameters used for ^{188}Pb .

$\alpha_1 = \beta_1$	$\alpha_2 = \beta_2$	Δ_1
8.5 keV	23.4 keV	1923 keV

all unperturbed levels. The knowledge of these unperturbed bands and their mixing matrix elements makes the process of configuration mixing in a nucleus more transparent than before. Starting from the experimental level energies, it is possible to deduce a set of unperturbed experimental bands using a phenomenological three-state [9,24,25] (or two-state [26,27]) band-mixing analysis. The comparison between the IBM unperturbed bands and these unperturbed experimental bands, together with the knowledge of the full energy spectrum and the $B(E2)$ values, forms an extensive test for the parameters that describe a certain isotope chain.

Starting from IBM parameters for the Pb isotopes as determined by Fossion *et al.* [23], a slightly different fit was performed. The parameters for \hat{H}_{reg} , \hat{H}_{2p-2h} , and \hat{H}_{4p-4h} remain unchanged, except for ε_{reg} , which was taken as 0.92 MeV instead of 0.90 MeV. The mixing parameters α_i and β_i were fixed in ^{196}Pb . The value for Δ_1 was obtained as the result of a fitting procedure for the Pb isotopes ($A = 186-196$). Basically Δ_1 was fitted for ^{186}Pb and ^{196}Pb and the Δ_1 for the other isotopes was chosen following a linear variation between $\Delta_1(^{186}\text{Pb})$ and $\Delta_1(^{196}\text{Pb})$. Then, the difference between the experimental 0_2^+ and the IBM 0_2^+ was taken for all isotopes considered and added to the corresponding Δ_1 . This method gives a better description of the slope of the energy levels through the isotope chain.

Moreover, the $\Delta_1(^{188}\text{Pb})$ obtained in this way is in good agreement with the theoretical prediction that makes use of experimental separation energies [17]. Since Δ_2 is associated with the unperturbed energy needed to excite $4p-4h$ configurations, the value was taken as $2 \cdot \Delta_1$ [28]. The parameters for ^{188}Pb are listed in Table I. The low-energy part of the resulting IBM spectrum for ^{188}Pb is presented in Fig. 1. Comparison with the experiment will be discussed in the next section.

By inspecting the unperturbed lowest bands (see left part of Fig. 1) one notices that mixing modifies the structure of the $2p-2h$ and $4p-4h$ 0^+ states and of the three 2^+ states because of the small energy differences between these unperturbed states (see Fig. 1). The mixing matrix elements between the first 0^+ state in each of the three unperturbed bands and between the first 2^+ state in each of the three unperturbed bands are given in Table II. The spin dependence of the absolute value of the mixing matrix elements can be seen from Fig. 2. The mixing matrix elements between the $J_i^+(N)$ and the $J_i^+(N+4)$ unperturbed states vanish because of the precise structure of the IBM mixing Hamiltonian [see Eqs. (4) and (5)]. For the sake of clearness, we stress that these mixing matrix elements can be compared with the mixing matrix elements used in more phenomenological calculations.

One can verify that a simple two-level mixing approximation for the unperturbed $0_1^+(N+2)$ and the unperturbed $0_1^+(N+4)$ states accurately reproduces the energies resulting from a full diagonalization of the Hamiltonian matrix (which

TABLE II. Mixing matrix elements between the first 0^+ and between the 2^+ state in each of the three unperturbed bands [see also Eq. (8)]. The matrix elements are expressed in MeV.

	$0_1^+(N)$	$0_1^+(N+2)$	$0_1^+(N+4)$
$0_1^+(N)$	0	-0.0768	0
$0_1^+(N+2)$	-0.0768	0	0.1908
$0_1^+(N+4)$	0	0.1908	0

	$2_1^+(N)$	$2_1^+(N+2)$	$2_1^+(N+4)$
$2_1^+(N)$	0	0.0711	0
$2_1^+(N+2)$	0.0711	0	0.1349
$2_1^+(N+4)$	0	0.1349	0

takes into account the interaction with the other 55 0^+ levels). This can also be seen in Table III, which gives the coefficients for the wave functions of the 0^+ (and 2^+) states resulting from the full diagonalization expressed in the unperturbed basis (8). Only the coefficients of the lowest three unperturbed 0^+ (and 2^+) states are shown. We point out that this severe two-level mixing approximation cannot reproduce the correct phase.

III. $B(E2)$ VALUES AND CONSTRUCTION OF COLLECTIVE BANDS

In the process of diagonalization of the full Hamiltonian (1) (excluding \hat{V}_{mix}) in the three subspaces separately, we have also made an ‘‘intermediate’’ calculation concerning $B(E2)$ values. The knowledge of the basis states (7) and (8) gives rise to two interesting expressions for the reduced matrix element of a transition between the initial $J_i(i)$ and final $J_f(f)$ state,

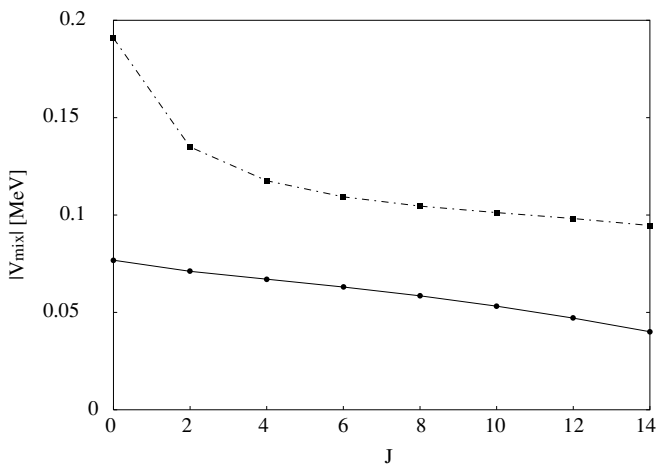


FIG. 2. Absolute value of the mixing matrix elements for the lowest J states in the three unperturbed bands [see also Eq. (8)]. The full line shows the absolute value of the mixing matrix elements between the $J_1^+(N)$ and the $J_1^+(N+2)$ states. The dot-dashed line shows the absolute value of the mixing matrix elements between the $J_1^+(N+2)$ and the $J_1^+(N+4)$ states (extended up to $J = 14$).

TABLE III. Coefficients for the wave functions of the 0^+ (and 2^+) states resulting from the full diagonalization expressed in the unperturbed basis (8). Only the coefficients of the lowest three unperturbed states $|0_1^+\rangle'_\nu$ and $|2_1^+\rangle'_\nu$ ($\nu = N, N+2, N+4$) are given.

	$ 0_1^+\rangle'_N$	$ 0_1^+\rangle'_{N+2}$	$ 0_1^+\rangle'_{N+4}$
$ 0_1^+\rangle$	-0.9897	-0.1310	0.0309
$ 0_2^+\rangle$	0.1216	-0.7624	0.6148
$ 0_3^+\rangle$	-0.0611	0.5893	0.7655

	$ 2_1^+\rangle'_N$	$ 2_1^+\rangle'_{N+2}$	$ 2_1^+\rangle'_{N+4}$
$ 2_1^+\rangle$	0.1907	-0.6379	0.7091
$ 2_2^+\rangle$	0.5964	-0.4906	-0.5664
$ 2_3^+\rangle$	0.7696	0.5114	0.2187

that is,

$$\begin{aligned}
 & \langle J_f, f || T(E2) || J_i, i \rangle \\
 &= \sum_k \sum_p a_{k,i}^v(J_i) a_{p,f}^v(J_f) \langle J_f, p || T(E2) || J_i, k \rangle_{\nu=N} \\
 &+ \sum_l \sum_q a_{l,i}^v(J_i) a_{q,f}^v(J_f) \langle J_f, q || T(E2) || J_i, l \rangle_{\nu=N+2} \\
 &+ \sum_m \sum_r a_{m,i}^v(J_i) a_{r,f}^v(J_f) \langle J_f, r || T(E2) || J_i, m \rangle_{\nu=N+4}
 \end{aligned} \tag{9}$$

and

$$\begin{aligned}
 & \langle J_f, f || T(E2) || J_i, i \rangle \\
 &= \sum_{k,p,s,s'} a_{k,i}^v(J_i) a_{p,f}^v(J_f) \tilde{b}_{s,k}^v(J_i) \tilde{b}_{s',p}^v(J_f) \\
 &\quad \times \langle J_f, s' || T(E2) || J_i, s \rangle'_{\nu=N} \\
 &+ \sum_{l,q,t,t'} a_{l,i}^v(J_i) a_{q,f}^v(J_f) \tilde{b}_{t,l}^v(J_i) \tilde{b}_{t',q}^v(J_f) \\
 &\quad \times \langle J_f, t' || T(E2) || J_i, t \rangle'_{\nu=N+2} \\
 &+ \sum_{m,r,u,u'} a_{m,i}^v(J_i) a_{r,f}^v(J_f) \tilde{b}_{u,m}^v(J_i) \tilde{b}_{u',r}^v(J_f) \\
 &\quad \times \langle J_f, u' || T(E2) || J_i, u \rangle'_{\nu=N+4},
 \end{aligned} \tag{10}$$

where the $\tilde{b}_{s,k}$ are the components of transposed matrix $\tilde{\mathbf{B}}$ of Eq. (8). Expression (10) is most interesting because it allows us to check which transitions in the unperturbed bands make up for an important contribution to a certain transition $J_i(i) \rightarrow J_f(f)$. We now apply the aforementioned method to the particular case of ^{188}Pb .

For ^{188}Pb , only two experimental $B(E2)$ values are known [11]:

$$B(E2; 2_1^+ \rightarrow 0_1^+) = 5(3) \text{ W.u.} \tag{11}$$

and

$$B(E2; 4_1^+ \rightarrow 2_1^+) = 160(80) \text{ W.u.} \tag{12}$$

In the calculation of the $E2$ transition rates, we use the consistent-Q procedure [29] to determine the $E2$ transition

TABLE IV. Parameters for $E2$ transitions in ^{188}Pb . The effective charges are expressed in $e \cdot b$, the χ are dimensionless.

χ_{reg}	χ_{2p-2h}	χ_{4p-4h}	e_{reg}	$e_{2p-2h} = e_{4p-4h}$
0	0.515	-0.680	0.110	0.132

operator as

$$T(E2) = \sum_{i=1}^3 e_i [(s^\dagger \tilde{d} + d^\dagger \tilde{s})^{(2)} + \chi_i (d^\dagger \tilde{d})^{(2)}]. \quad (13)$$

So we choose the values for χ_{2p-2h} and χ_{4p-4h} as obtained in [23] and fit the effective charges to those two known data. We took e_{2p-2h} and e_{4p-4h} to be 1.2 times e_{reg} . Table IV lists the parameters used. We point out that we have chosen $\chi_{\text{reg}} = 0$. We made this choice because there are no data available for transitions within the regular band; hence we are unable to fit χ_{reg} to known experimental values. Evidently, the ground state is regular and we know the $B(E2)$ value for the $2_1^+ \rightarrow 0_1^+$ transition, but as χ_{reg} has no influence on $2^+ \rightarrow 0^+$ transitions in the U(5) limit, we cannot make use of this transition in determining χ_{reg} .

For this choice of parameters the IBM fit yields the following results:

$$B(E2; 2_1^+ \rightarrow \text{g.s.}) = 0.0195 (e b)^2 \text{ or } 3 \text{ W.u.} \quad (14)$$

and

$$B(E2; 4_1^+ \rightarrow 2_1^+) = 0.9747 (e b)^2 \text{ or } 152 \text{ W.u.} \quad (15)$$

In the remaining part of the discussion, we use the fitted effective charges to make further theoretical predictions.

We now come to the question of labeling the mixed states, resulting from diagonalization of the full Hamiltonian (1),

TABLE V. Interband transitions involving the 2_3^+ state.

Transition	$B(E2)$ value (W.u.)
$4_2^+ \rightarrow 2_3^+$	44
$2_3^+ \rightarrow 2_1^+$	36
$2_3^+ \rightarrow 2_2^+$	2

in a meaningful way into a given band. As a criterion, we start from the calculated high-spin members of the two bands and follow the $E2$ decay. The particular $E2$ decay sequence down to low spin, for which the intraband $B(E2)$ values are bigger than the interband $B(E2)$ values, are placed in a given collective band. The results are shown in Fig. 3. The IBM 2_3^+ level at 969 keV is not shown in Fig. 3 and all interband transitions involving this state can be found in Table V. The transitions between Bands II and III in Fig. 3 that are not shown are less than 1 W.u. The 725-keV 0^+ state [30] in Fig. 3 is indicated with a dashed line and tentative energy. The 0_3^+ level was identified in two experimental studies [24,30], but recently performed experiments [9,12] do not yield conclusive evidence for this state and its energy. In Table VI, we present the magnitudes (given in percentage) of the three different configurations within the three bands (I, II, and III). From inspecting Table VI, it becomes clear that a good separation in different subspaces N , $N + 2$, and $N + 4$ ceases to hold on the basis of the mixing percentages for the low-spin 0^+ and 2^+ members. Using the reduced $E2$ matrix elements as a guiding principle, as discussed before, one arrives at the results shown in Fig. 3. So one needs both the mixing percentages and the $B(E2)$ values to obtain a good understanding of the nature of the bands.

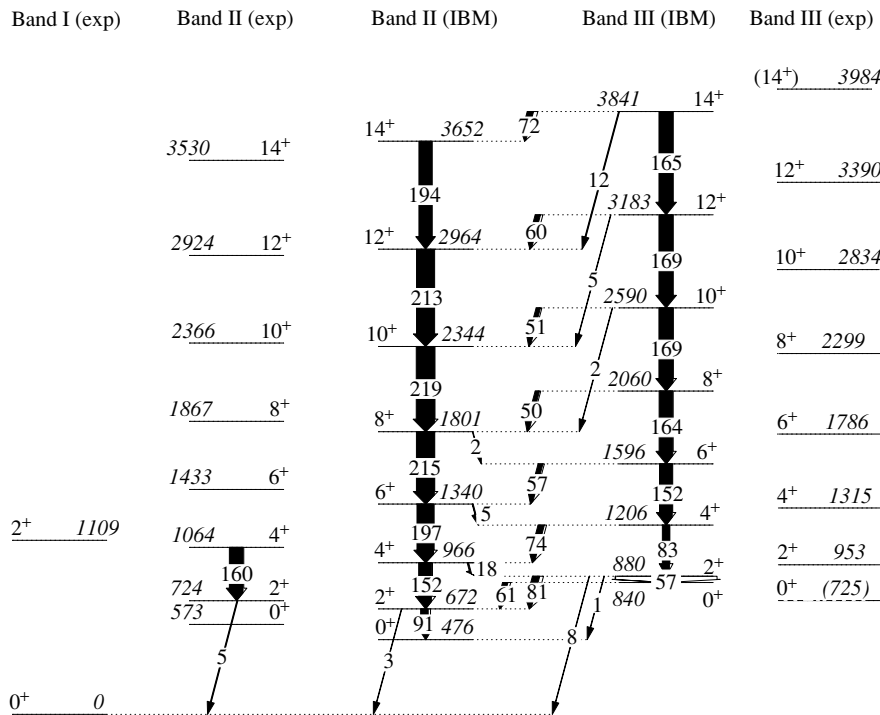


FIG. 3. Experimental and theoretical level scheme in ^{188}Pb . The arrows denote the $B(E2)$ values for a given transition, expressed in Weisskopf units. The experimental data were taken from [9,11,13,30].

TABLE VI. The magnitudes (given in percentages) of the three different configurations (N , $N + 2$, and $N + 4$) in the constructed bands.

	Band I			Band II			Band III				
	N	$N+2$	$N+4$	N	$N+2$	$N+4$	N	$N+2$	$N+4$		
0_1^+	98	2	0	0_2^+	2	59	40	0_3^+	0	38	62
2_3^+	59	32	8	2_1^+	4	44	52	2_2^+	36	30	35
				4_1^+	0	30	70	4_2^+	1	71	28
				6_1^+	0	23	77	6_2^+	0	78	22
				8_1^+	0	20	80	8_2^+	0	80	20
				10_1^+	0	21	79	10_2^+	0	79	21
				12_1^+	0	26	74	12_2^+	0	74	26
				14_1^+	0	40	60	14_2^+	0	61	39

Comparing the IBM results with the experimental bands, we notice that the structure of the collective bands is reproduced rather well. The energy levels that constitute the more collective Band II are in good agreement with the experimental results. The structure of Band III is also described rather well, although the value of Δ_{2p-2h} seems a bit too small and the mixing parameter between the two intruder configurations seems slightly too large.

When we take a closer look at the $E2$ transitions between the low-lying levels, something interesting occurs. Using expression (10), one can single out those contributions of the reduced matrix elements for the transitions in the unperturbed bands that make up the major contribution to a given transition $J_i(i) \rightarrow J_f(f)$ with the condition that their sum may not deviate more than 10% from the total value with all contributions taken into account. In the case of ^{188}Pb , it turns out that, for the so-constructed Bands II and III, the main contribution to intraband transitions always consists of the term with the corresponding lowest rank transition in the unperturbed 2p-2h band and the one in the unperturbed 4p-4h band. Thus

$$\begin{aligned}
 & \langle J_f, f || T(E2) || J_i, i \rangle \\
 & \cong \sum_{l,q} a_{l,i}^{N+2}(J_i) a_{q,f}^{N+2}(J_f) \tilde{b}_{1,l}^{N+2}(J_i) \tilde{b}_{1,q}^{N+2}(J_f) \\
 & \quad \times \langle J_f, 1 || T(E2) || J_i, 1 \rangle'_{N+2} \\
 & + \sum_{m,r} a_{m,i}^{N+4}(J_i) a_{r,f}^{N+4}(J_f) \tilde{b}_{1,m}^{N+4}(J_i) \tilde{b}_{1,r}^{N+4}(J_f) \\
 & \quad \times \langle J_f, 1 || T(E2) || J_i, 1 \rangle'_{N+4} \\
 & = R(N+2) \langle J_f, f || T(E2) || J_i, i \rangle + R(N+4) \\
 & \quad \times \langle J_f, f || T(E2) || J_i, i \rangle \quad (16)
 \end{aligned}$$

where $|J_i, i\rangle$ and $|J_f, f\rangle$ are both states in Band II or both states in Band III. This fact is as expected. More interesting is the ratio R of those two main contributions to the total value of the reduced matrix element, because they are related to the ‘‘purity’’ of a certain transition. These results are depicted in Fig. 4.

Notice that the ratio $R(N+4)$ becomes larger than the ratio $R(N+2)$ for the $2_2^+ \rightarrow 0_3^+$ transition in Band III. This

very large ratio $R(N+4)$ for the $2_2^+ \rightarrow 0_3^+$ transition in Band III is due to the combined effect of the large mixing and the relative magnitudes of the two contributing reduced matrix elements (16).

IV. $E0$ TRANSITIONS

Within the IBM, a reduced form of the $E0$ operator [i.e., $\hat{\rho}(E0) \equiv \hat{T}(E0)/eR_0^2$] can be defined as

$$\hat{\rho}(E0) = [\alpha_1 \hat{N} + \beta_1 \hat{n}_d]_{\text{reg}} + [\alpha_2 \hat{N} + \beta_2 \hat{n}_d]_{\text{intr}}, \quad (17)$$

where we have chosen, similarly as for the $E2$ values, equal parameters for the two intruder configurations. With this definition, the α_i and β_i are dimensionless. If one wants to relate them to the equivalent parameters expressed in $e \cdot \text{fm}^2$, as used in [31], one has to multiply them by eR_0^2 .

Because a least-square fit of these parameters to the known ρ^2 values in ^{188}Pb [9] does not impose enough constraints on the problem, we also include the isotopic shifts $\Delta \langle r^2 \rangle^{A,208}$, recently determined by De Witte *et al.* [32] for the Pb isotopes in the fit. Therefore, we rewrite the expression for the nuclear radius within the IBM [18,33] as

$$r^2 = r_c^2 + eR_0^2 \langle \hat{\rho}(E0) \rangle. \quad (18)$$

Performing a fit to the combination of the values $\Delta \langle r^2 \rangle^{A,208}$ (for $A = 186-196$) and the ρ^2 values for the $8_2^+ \rightarrow 8_1^+$, $6_2^+ \rightarrow 6_1^+$, $4_2^+ \rightarrow 4_1^+$, and $2_2^+ \rightarrow 4_1^+$ $E0$ transitions results in the following parameter values:

$$\begin{aligned}
 \alpha_1 &= -0.0020, & \beta_1 &= 0.800, \\
 \alpha_2 &= -0.0086, & \beta_2 &= 0.183.
 \end{aligned}$$

The corresponding values for ρ^2 are given in Table VII. The values for the transitions between the 0^+ states, which were not included in the fitting procedure, deviate considerably from the experimental values, in contrast to the good agreement obtained for the other ρ^2 values and for the $\Delta \langle r^2 \rangle^{A,208}$ isotopic shifts. The large ρ^2 value for the $0_3^+ \rightarrow 0_2^+$ transition seems to suggest that the mixing between the 2p-2h and the 4p-4h configurations resulting from our present study is still somewhat too large compared with the experimental results [9]. We aim at a more thorough study of $E0$ properties (isotopic and isomeric shifts, $E0$ transitions, etc.) in the whole Pb region to gain a better understanding of the mixing and of the deduced parameters.

V. COMPARISON WITH THE COLLECTIVE ROTATIONAL MODEL

Having constructed two different collective bands starting from the IBM and using the prescription to define bands on the basis of the calculated $B(E2)$ values, we now need to check for consistency with the results of other theoretical approaches. First, we concentrate on the quadrupole moments.

Within the IBM, the quadrupole moments are calculated as

$$Q(J) = \sqrt{\frac{16\pi}{5}} \langle JJ | T(E2, 0) | JJ \rangle. \quad (19)$$

From the point of view of the collective rotational model [34–36], the electric quadrupole moment is defined as

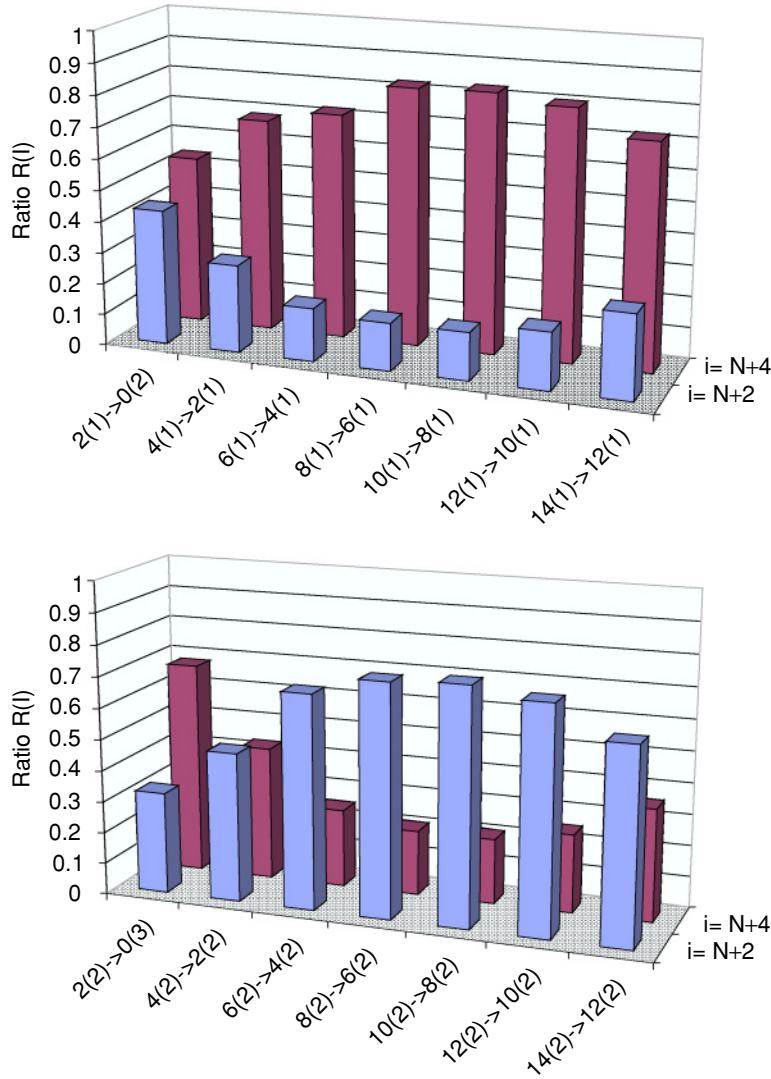


FIG. 4. (Color online) The top part shows the ratios $R(N+2)$ and $R(N+4)$ [see Eq. (16)] for the intraband transitions in Band II; the bottom part shows the ratios $R(N+2)$ and $R(N+4)$ for the intraband transition in Band III.

$$Q = \sqrt{\frac{16\pi}{5}} \langle J, K, M = J | \mathcal{M}(E2, 0) | J, K, M = J \rangle. \quad (20)$$

For $K = 0$ bands this reduces to

$$Q = \frac{-J(J+1)}{(J+1)(2J+3)} Q_0^0, \quad (21)$$

TABLE VII. Comparison between the experimental and calculated monopole transition ρ^2 values. The experimental values were taken from [9]. In Ref. [9] a ρ^2 value of approximately 0.025 is given for the $E0$ decay from the 0_3^+ state.

Transition	ρ^2 (IBM)	ρ^2 (exp.)
$8_2^+ \rightarrow 8_1^+$	0.0107	0.012
$6_2^+ \rightarrow 6_1^+$	0.0150	0.016
$4_2^+ \rightarrow 4_1^+$	0.0214	0.027
$2_2^+ \rightarrow 2_1^+$	0.0118	0.010
$0_2^+ \rightarrow 0_1^+$	2.4×10^{-4}	0.007
$0_3^+ \rightarrow 0_1^+$	8.1×10^{-5}	—
$0_3^+ \rightarrow 0_2^+$	0.0623	—

with the intrinsic quadrupole moment Q_0^0 defined as

$$Q_0^0 = \sqrt{\frac{16\pi}{5}} \langle K = 0 | \mathcal{M}(E2, 0) | K = 0 \rangle. \quad (22)$$

Equating the quadrupole moments of Eqs. (19) and (21) allows us to extract an equivalent intrinsic quadrupole moment Q_0^0 assuming $K = 0$ bands. Likewise one can use the IBM $B(E2)$ values to extract an equivalent intrinsic quadrupole moment Q_0^0 using the collective rotational model $B(E2)$ expression

$$B(E2; J+2, K=0 \rightarrow J, K=0) = \frac{5}{16\pi} (2J+1) \begin{pmatrix} J+2 & 2 & J \\ 0 & 0 & 0 \end{pmatrix}^2 (Q_0^0)^2. \quad (23)$$

Having extracted an intrinsic quadrupole moment, one can deduce a deformation parameter β_0 using the expression

$$Q_0 = \frac{3ZR_0^2}{\sqrt{5\pi}} \beta_0. \quad (24)$$

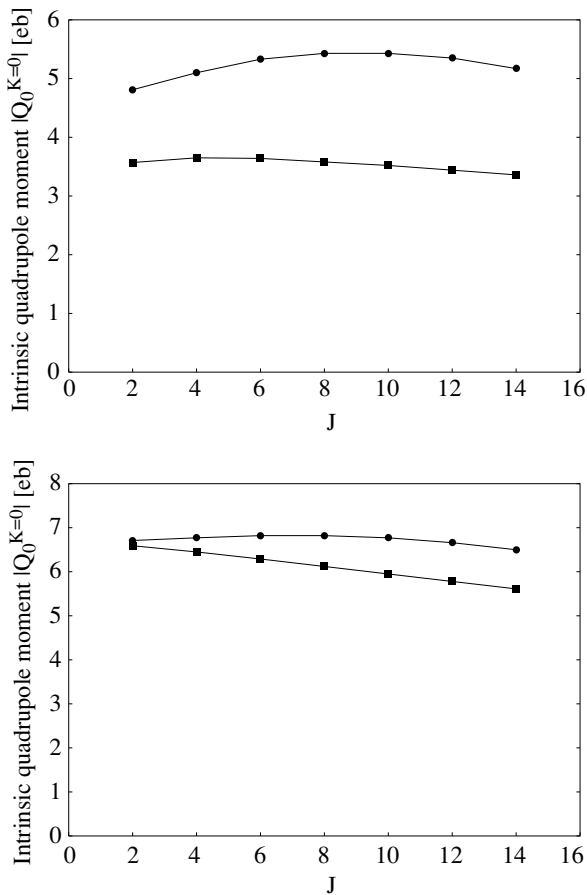


FIG. 5. The upper plot shows the comparison between the magnitudes of the intrinsic quadrupole moments extracted from the theoretical $B(E2)$ values (\bullet) and the magnitudes of the intrinsic quadrupole moments extracted from the diagonal matrix elements (\blacksquare), both for the unperturbed 2p-2h band. The lower plot shows the same comparison for the unperturbed 4p-4h band.

If one wants to extract collective model parameters starting from the bands constructed within the IBM, one needs to test the assumption to treat them as $K = 0$ collective bands. If the interpretation of a $K = 0$ band characterized by a single Q_0^0 value is to make sense, one expects that values of Q_0^0 extracted using these two procedures [equating IBM results with the collective rotational model results, given in Eqs. (21) and (23)] will not differ much. Moreover, one expects only a moderate variation of Q_0^0 as a function of J along the band. In Fig. 5 we show the comparison between the intrinsic quadrupole moments extracted from the $B(E2)$ values (23) and the absolute values of the intrinsic quadrupole moments extracted using Eq. (21). This comparison is presented for the unperturbed 2p-2h band (upper part) and for the unperturbed 4p-4h band (lower part). One notices that the unperturbed 4p-4h band exhibits a $K = 0$ rotational-like behavior to a large extent and can be characterized by a single intrinsic structure. For the 2p-2h band there are distinct differences between the intrinsic quadrupole moments extracted using the two methods. Because the parameters for the unperturbed 4p-4h band were fixed using I-spin symmetry [23], we can explain the $K = 0$ rotational behavior of this band by comparing with

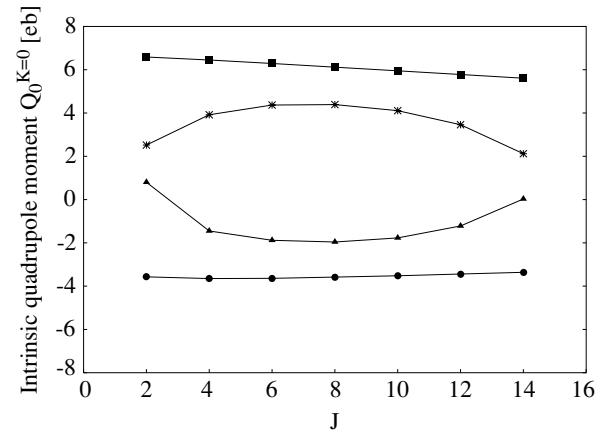


FIG. 6. Intrinsic quadrupole moment extracted from transition matrix elements, calculated within the IBM. The intrinsic quadrupole moment is expressed in $e \cdot b$. Results for the 2p-2h unperturbed band are represented with \bullet ; results for the 4p-4h unperturbed band with \blacksquare . Bands II and III are represented, respectively, by $*$ and \blacktriangle .

the ground state band in ^{180}W , which is recognized as a $K = 0$ rotational band [37]. Moreover, one notices that the intrinsic quadrupole moments stay approximately constant for the unperturbed bands. This is also reflected in the approximately constant behavior of the intraband $B(E2)$ values as a function of spin for the higher spin states in Fig. 3.

We can also extract the sign of the intrinsic quadrupole moment and the deformation parameter. Therefore we have plotted in Fig. 6 the intrinsic quadrupole moment Q_0^0 derived from the $E2$ diagonal matrix elements (21). The intrinsic quadrupole moments of the unperturbed 4p-4h band are positive, indicating a prolate deformation of the nucleus, whereas the negative sign of the intrinsic quadrupole moments in the unperturbed 2p-2h band is consistent with an oblate deformation. The extracted values are in good agreement with the magnitudes of the quadrupole moments reported by Dracoulis *et al.* [9].

Using Eq. (24), we obtain the deformation parameter β_0 . For the unperturbed 2p-2h band, β_0 varies between -0.11 and -0.12 , whereas for the unperturbed 4p-4h band, β_0 varies between 0.19 and 0.22 . These values are smaller than the deformation parameters calculated by Bender *et al.* [10] using self-consistent mean-field methods.

VI. CONCLUSION

In the present paper we have carried out a detailed analysis of the presence of various families of collective bands, in particular for ^{188}Pb . We have started from an algebraic model approach (the interacting boson model) to truncate the extended shell-model space that incorporates the presence of proton particle-hole excitations across the $Z = 82$ closed shell. Moreover, making use of a concept called intruder symmetry, we have been able to reduce the number of parameters in the present description. A first calculation has been carried out by Fossion *et al.* [23], accentuating the presence of three different families. Here, we have defined an intermediate

basis that defines three separate systems by diagonalizing the Hamiltonian in the 0p-0h, 2p-2h, and 4p-4h configuration spaces separately. This basis allows us to understand the mixing between the unperturbed bands in a transparent way. Moreover, we have used the $E2$ decay, starting at high spin, to define “physical” bands also progressing to low-spin members. Here the conclusion points toward an important mixing between the $0_2^+, 0_3^+$ and the $2_1^+, 2_2^+$, and 2_3^+ band members, still allowing the separation into two collective band structures. A simple reanalysis of these two bands within the collective rotational model is consistent with prolate and oblate band characteristics for the unperturbed 4p-4h and 2p-2h bands, respectively. Extracted magnitudes of the intrinsic quadrupole and the deformation parameters are in good agreement with calculations starting from mean-field approaches. We have also calculated monopole transition ρ^2 values. The fitted parameters give a good description of the $\Delta\langle r^2 \rangle^A$ values for the $A = 186\text{--}196$ Pb isotopes and of the experimental ρ^2 values. Deviations of the calculated ρ^2 values from the experimental ones for the 0^+ states point out that two constructed bands are still somewhat overmixed.

It is our aim to carry out a similar analysis for the other Pb nuclei near the neutron midshell region and follow the mixing patterns between the two bands when moving away from the midshell region (at $N = 104$) and to incorporate an extensive study of electromagnetic properties ($E2$ and $E0$ transitions) and the study of isotopic and isomeric shifts as well.

ACKNOWLEDGMENTS

The authors are most grateful to G. Dracoulis and R. Julin for extensive discussions, to P. Van Isacker for discussions on $E0$ transitions, and to R. Janssens, R. Page, A. Andreyev, and A. Dewald for comments on the manuscript. They would also like to thank P.-H. Heenen, M. Bender, P. Van Duppen, and J. L. Wood for their continuous interest in this research. Financial support from the “FWO-Vlaanderen” (V.H. and K.H.), the University of Ghent (S.D.B. and K.H.), and the IWT (R.F.), as well as from the OSTC (Grant IUAP #P5/07), is acknowledged.

-
- [1] K. Heyde, P. Van Isacker, M. Waroquier, J. L. Wood, and R. A. Meyer, *Phys. Rep.* **102**, 291 (1983).
- [2] J. L. Wood, K. Heyde, W. Nazarewicz, M. Huyse, and P. Van Duppen, *Phys. Rep.* **215**, 101 (1992).
- [3] R. Julin, K. Helariutta, and M. Muikku, *J. Phys. G* **27**, R109 (2001).
- [4] A. N. Andreyev *et al.*, *Nature* **405**, 430 (2000).
- [5] A. Frank, P. Van Isacker, and C. E. Vargas, *Phys. Rev. C* **69**, 034323 (2004).
- [6] M. Bender, P. Bonche, T. Duguet, and P.-H. Heenen, *Phys. Rev. C* **69**, 064303 (2004).
- [7] R. R. Rodríguez-Guzmán, J. L. Egidio, and L. M. Robledo, *Phys. Rev. C* **69**, 054319 (2004).
- [8] J. L. Egidio, L. M. Robledo, and R. R. Rodríguez-Guzmán, *Phys. Rev. Lett.* **93**, 082502 (2004).
- [9] G. D. Dracoulis *et al.*, *Phys. Rev. C* **69**, 054318 (2004).
- [10] M. Bender, P.-H. Heenen, and P.-G. Reinhard, *Rev. Mod. Phys.* **75**, 121 (2003).
- [11] A. Dewald *et al.*, *Phys. Rev. C* **68**, 034314 (2003).
- [12] K. Van de Vel *et al.*, *Phys. Rev. C* **68**, 054311 (2003).
- [13] G. D. Dracoulis *et al.*, *Phys. Rev. C* **67**, 051301(R) (2003).
- [14] W. Reviol, C. J. Chiara, O. Pechenaya, D. G. Sarantites, P. Fallon, and A. O. Macchiavelli, *Phys. Rev. C* **68**, 054317 (2003).
- [15] N. A. Smirnova, P.-H. Heenen, and G. Neyens, *Phys. Lett.* **B569**, 151 (2003).
- [16] T. Duguet, M. Bender, P. Bonche, and P.-H. Heenen, *Phys. Lett.* **B559**, 201 (2003).
- [17] K. Heyde, J. Jolie, J. Moreau, J. Ryckebusch, M. Waroquier, P. Van Duppen, M. Huyse, and J. L. Wood, *Nucl. Phys.* **A466**, 189 (1987).
- [18] F. Iachello and A. Arima, *The Interacting Boson Model* (Cambridge University Press, Cambridge, England/London/New York, 1987).
- [19] A. Frank and P. Van Isacker, *Algebraic Methods in Molecular and Nuclear Structure Physics* (Wiley, New York, 1994).
- [20] P. D. Duval and B. R. Barrett, *Nucl. Phys.* **A376**, 213 (1982).
- [21] R. Bengtsson and W. Nazarewicz, *Z. Phys. A* **334**, 269 (1989).
- [22] W. Nazarewicz, *Phys. Lett.* **B305**, 195 (1993).
- [23] R. Fossion, K. Heyde, G. Thiamova, and P. van Isacker, *Phys. Rev. C* **67**, 024306 (2003).
- [24] R. G. Allatt *et al.*, *Phys. Lett.* **B437**, 29 (1998).
- [25] R. D. Page *et al.*, in *Proceedings of the 3rd International Conference on Exotic Nuclei and Atomic Masses ENAM, Hämeenlinna, Finland, July 2001*, edited by J. Äystö, P. Dendooven, A. Jokinen, and M. Leino (Springer-Verlag, Berlin/Heidelberg, 2003), p. 309.
- [26] G. D. Dracoulis, *Phys. Rev. C* **49**, 3324 (1994).
- [27] G. D. Dracoulis, A. P. Byrne, and A. M. Baxter, *Phys. Lett.* **B432**, 37 (1998).
- [28] K. Heyde, J. Schietse, and C. De Coster, *Phys. Rev. C* **44**, 2216 (1991).
- [29] D. D. Warner and R. F. Casten, *Phys. Rev. C* **28**, 1798 (1983).
- [30] Y. Le Coz *et al.*, *EPJdirect A* **3**, 1 (1999).
- [31] J. L. Wood, E. F. Zganjar, C. De Coster, and K. Heyde, *Nucl. Phys.* **A651**, 323 (1999).
- [32] H. De Witte *et al.* (private communication and to be published).
- [33] M. K. Harder, K. T. Tang, and P. Van Isacker, *Phys. Lett.* **B405**, 25 (1997).
- [34] A. Bohr and B. R. Mottelson, *Nuclear Structure* (Benjamin, Reading, MA, 1975), Vol. II.
- [35] W. Greiner and J. A. Maruhn, *Nuclear Models* (Springer-Verlag, Berlin/Heidelberg/New York, 1996).
- [36] D. J. Rowe, *Nuclear Collective Motion (Models and Theory)* (Methuen, London/New York, 1970).
- [37] E. Browne, *Nucl. Data Sheets* **71**, 81 (1994).